Supplementary Information

Structure and Rheology of Dual-Associative Protein Hydrogels Under Nonlinear Shear Flow

Michelle K. Sing, Matthew J. Glassman, Xenanthia T. Vronay-Ruggles, Wesley R. Burghardt, and Bradley D. Olsen*

Table of Contents

S.1: Rheo-SAXS Setup

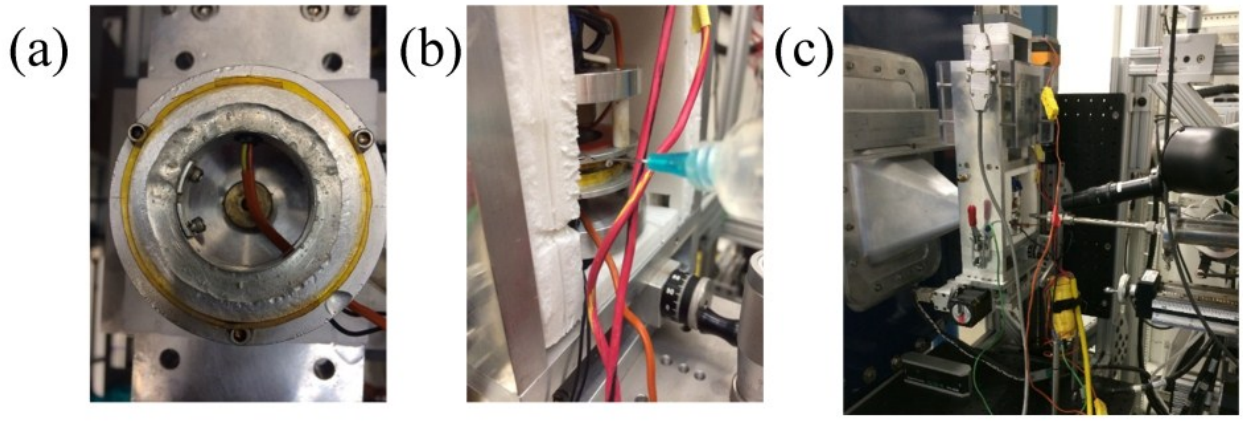

Figure S1.1: Example images during sample loading of the Rheo-SAXS shear cell. (a) Top view of sample loading onto a lower plate that was held at approximately 0 °C under an active supply of LN_2-chilled N_2 gas. Note that the Kapton® barrier (orange) is already installed. (b) Insulated chamber with motor assembly installed and chamber windows open. Sample has been loaded and geometry is in the measuring position. Image was taken during application of mineral oil barrier

onto the exposed sample edges via syringe. (c) View of assembled shear cell in position between the source (right side) and the detector chamber (left side).

S.2: Anisotropy Calculations and Background Subtraction

The anisotropy parameter (Δ) and angle (χ) were calculated following the equations used by Caputo et al. such that:[1]

$$\Delta = \frac{\sqrt{\left(\left\langle \hat{q}_x{}^2 \right\rangle - \left\langle \hat{q}_y{}^2 \right\rangle\right)^2 + 4\left\langle \hat{q}_x \hat{q}_y \right\rangle^2}}{\left\langle \hat{q}^2 \right\rangle_o} \qquad \text{* MERGEFORMAT (1)}$$

$$2\chi = -\frac{180}{\pi}\tan^{-1}\left(\frac{2\left\langle \hat{q}_x \hat{q}_y \right\rangle}{\left\langle \hat{q}_x{}^2 \right\rangle - \left\langle \hat{q}_y{}^2 \right\rangle}\right) \qquad \text{* MERGEFORMAT (2)}$$

The weighted averages of intensity in x (flow) and y (gradient) directions $\left\langle \hat{q}_x{}^2 \right\rangle$ and $\left\langle \hat{q}_y{}^2 \right\rangle$ in equations * MERGEFORMAT (1) and * MERGEFORMAT (2) are calculated via the relation

$$\left\langle \hat{q}\hat{q} \right\rangle = \sum\sum \hat{q}\hat{q}\hat{S}_o\left(\hat{q}\right) d\hat{q}_x d\hat{q}_y \qquad \text{* MERGEFORMAT (3)}$$

where $\hat{S}_o$ represents the normalized intensity distribution from scattering, and $d\hat{q}_x$ and $d\hat{q}_y$ represent the pixel size in *q*-space. Translation to *q*-space was done using a sample-to-detector distance of 3,616.6mm, a wavelength of 0.0886nm, a pixel size of 0.1720mm, and the pixel location of the beam center as x = 752.5 and y = 186.994. The denominator in equation * MERGEFORMAT (1) is used to self-normalize each individual image.

The negative sign in equation * MERGEFORMAT (2) corrects for the direction of flow relative to the detector. The shear cell used rotates in the counterclockwise direction when viewed from directly above. Relative to the beam, the samples were sheared from right to left (Figure 1).

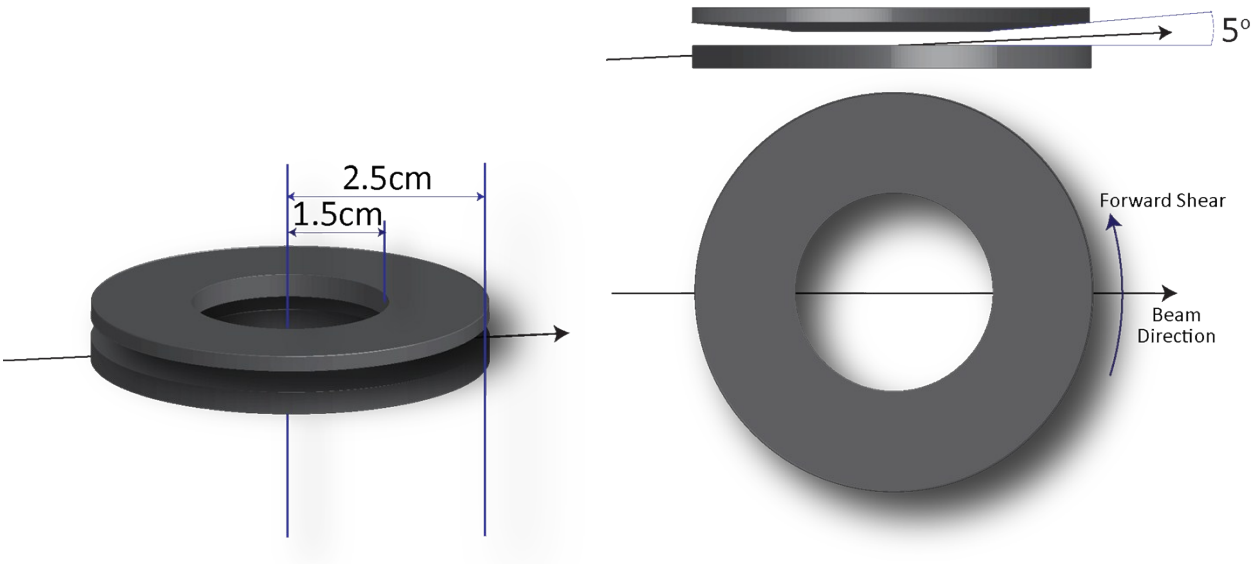

Figure S2.1: Schematic representation of shear cell used in scattering experiments showing direction of beam relative to the direction of flow.

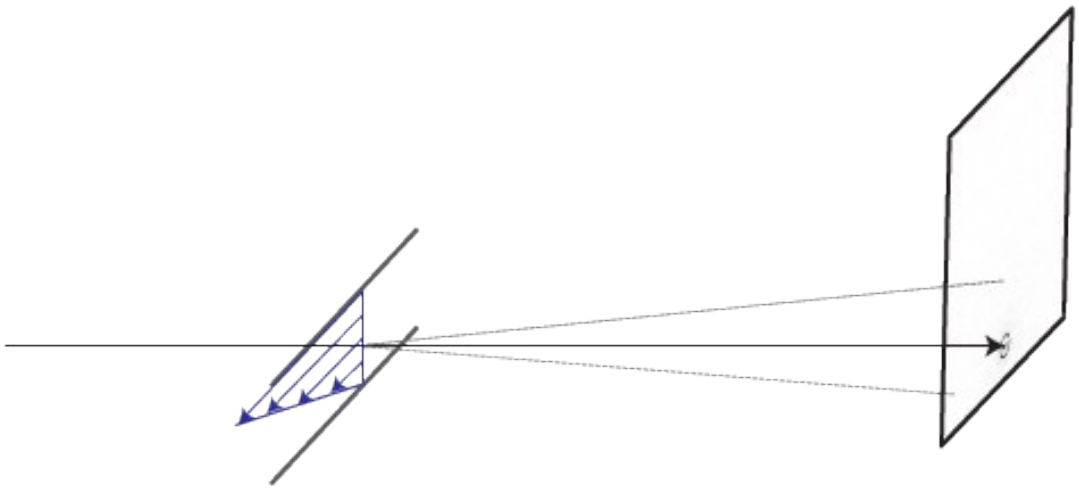

Figure S2.2: Beam direction relative to shear direction.

Prior to performing the above calculations, each image was background corrected using the equation

$$I(q) = \frac{I_{sample}}{T_{sample}} - \frac{t_{sample}}{t_{empty}} \frac{I_{empty}}{T_{empty}} \qquad \text{* MERGEFORMAT (4)}$$

where I, t, and T represent the intensity, sample time, and transmission of the sample and the background (empty). Following background correction, it was necessary to minimize the effect of the beam stop, and the lines of zero intensity and flares caused by the presence of air bubbles added additional noise to the data. Areas covered by the beam stop were filled in using centro-symmetry

and the data was cut off at values of q greater than 0.5 nm^{-1} in order to avoid the edge of the detector. Any data point for which the set of points [(q_x, q_y) (-q_x, q_y) (q_x, -q_y) (-q_x, -q_y)] could not be completely reconstructed was excluded from the analysis, as such incomplete sets introduce artificial bias into the calculation.

S.3: Percus-Yevick Fits and Bridging in Gels

Quiescent SAXS data was fit to the Percus-Yevick model for disordered hard spheres[2-3] using non-linear least squares fits:

$$I(q) = K \cdot S(q) F(q) + C \qquad \text{* MERGEFORMAT (5)}$$

S(q) represents the structure factor, calculated using the formula:

$$S(q) = \frac{1}{1 + 24\eta G(2qR)} \qquad \text{* MERGEFORMAT (6)}$$

where η represents the micelle packing fraction and R represents the hard sphere radius. The function G(x) is:

$$G(x) = \frac{a}{x^3}(\sin x - x\cos x) + \frac{\beta}{x^4}\left[2x\sin x + (2 - x^2)\cos x - 2\right] + \frac{\gamma}{x^6}\left(-x^4\cos x + 4\left[(3x^2 - 6)\cos x + (x^3 - 6x)\sin x + 6\right]\right) \qquad \text{* MERGEFORMAT (7)}$$

where the constants α, β, and γ reflect constants dependent upon the value of η:

$$\alpha = \frac{(1+2\eta)^2}{(1-\eta)^4}, \beta = -6\eta\frac{(1+\eta/2)^2}{(1-\eta)^4}, \gamma = \frac{\eta}{2}\frac{(1+2\eta)^2}{(1-\eta)^4} \qquad \text{* MERGEFORMAT (8)}$$

The form factor *F(q)* in equation * MERGEFORMAT (5) was calculated for polydisperse spheres:

$$F(q) = \frac{\int P(r) f^2(q,r)\, dr}{\int P(r)\, dr} \qquad \text{* MERGEFORMAT (9)}$$

where *P(r)* represents the lognormal probability distribution:

$$P(r) = \sqrt{2\bar{\sigma}_P^2 \pi}\exp\left[\frac{(-\ln r - \bar{r}_o)^2}{2\bar{\sigma}_P^2}\right] \qquad \text{* MERGEFORMAT (10)}$$

and $f(q,r)$ for a single sphere:

$$f(q,r) = \frac{4}{3}\pi r^3 \frac{3}{(qr)^3}(\sin qr - qr\cos qr). \qquad \text{* MERGEFORMAT (11)}$$

The expected value (r_o) and standard deviation (σ_P) represent the core radius and core radii distribution, respectively and can be calculated from the distribution as:

$$r_o = \exp\left(\bar{r}_o + \frac{1}{2}\bar{\sigma}_P^2\right) \rightarrow \bar{r}_o = \ln r_o - \frac{1}{2}\ln\left[\left(\frac{\sigma_P}{r_o}\right)^2 + 1\right] \text{ * MERGEFORMAT (12)}$$

$$\sigma_P = r_o\sqrt{\exp\bar{\sigma}_P^2 - 1} \rightarrow \bar{\sigma}_P = \sqrt{\ln\left[\left(\frac{\sigma_P}{r_o}\right)^2 + 1\right]} \text{ .* MERGEFORMAT (13)}$$

It should be noted that when r_o and σ_P are entered as parameters, it is necessary to pass $\bar{r}_o$ and $\bar{\sigma}_P$ to the form factor function using the transformed equations shown to the right of the arrows in * MERGEFORMAT (12) and * MERGEFORMAT (13).

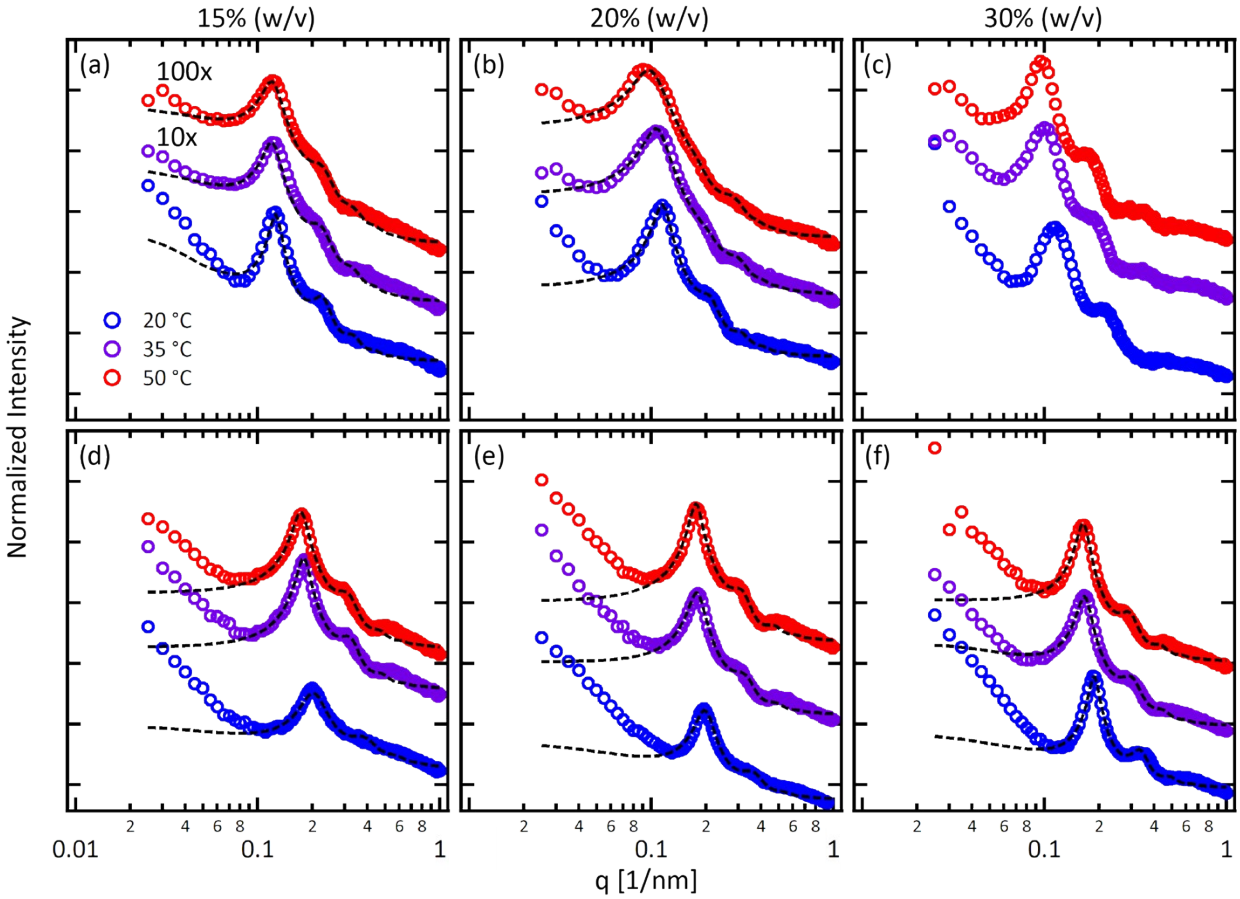

Figure S3.1: Background-corrected 1-D reductions of quiescent data for the diblock (a - c) and triblock (d - f) as a function of temperature and concentration. Intensities at 35C have been shifted by 10x. Intensities at 50C have been shifted by 100x. Black dashed lines indicate Percus-Yevick fits to data. Note that (c) does not contain corresponding fit data as the Percus-Yevick fit does not apply to the diblock at 30% (w/v) due to the formation of anisotropic microstructure suggested by birefringence. The upturn in intensity at low q indicates some larger length scale concentration

inhomogeneity that is common in many types of gels, although these gels have high optical transmission and there is no visible sign of macrophase separation.

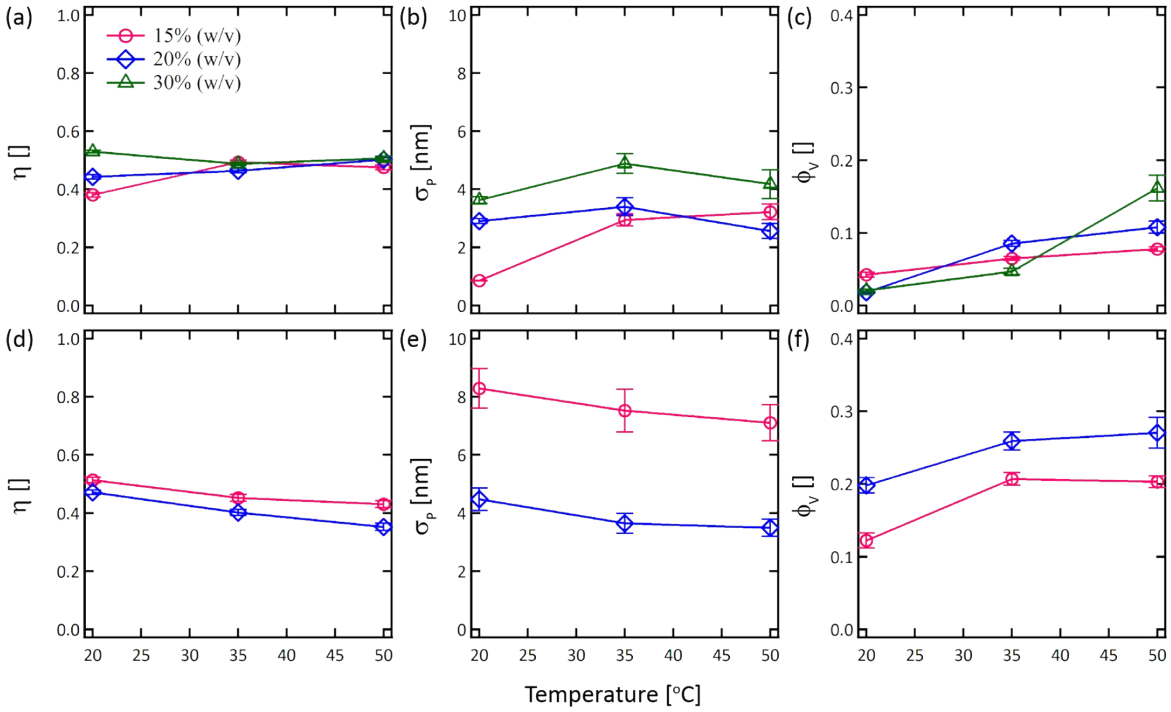

Figure S3.2: Additional Percus-Yevick fit parameters η and σ_P and the volume fraction of the core (ϕ_V) for $G_{10}P_4G_{10}$ (a-c) and $G_{20}P_4$ (d-f) showing temperature and concentration dependence of fit parameters (a,b,d,e) and micellar reinforcement as a function of core fraction (c,f). Values for the dispersity and core fraction are lower for the triblock than the diblock, and the micelle packing fraction does not have an apparent trend relative to the block architecture.

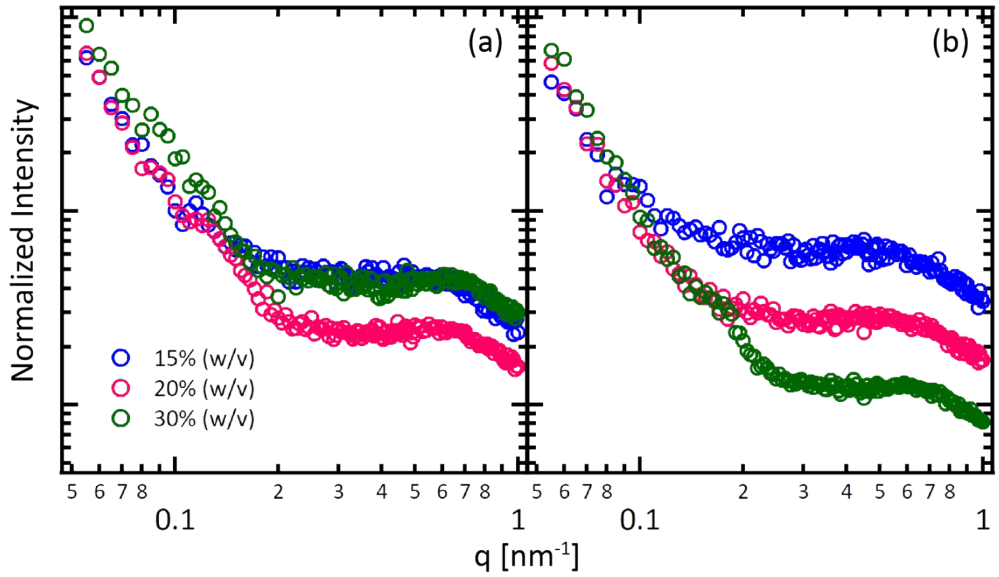

Figure S3.3: Background-corrected 1-D scattering profiles of both (a) diblock and (b) triblock proteins across all three concentrations used in this study at approximately 5 °C (well below the transition temperatures).

The fraction of bridged chains in the quiescent state can be estimated using the theoretical formulation of Semenov and Rubinstein.[4] The portion of micellar strands acting as bridged chains is proportional to $\phi^{0.14}/m$, where ϕ is the concentration of the system and m is the aggregation number.[4] Assuming the number of chains per aggregate falls between 20 and 50 and given the concentrations used in this work, the bridging chains should comprise 1 to 5% of the system (assuming no dangling chains are present).

S.4: Transient Deformation Behavior

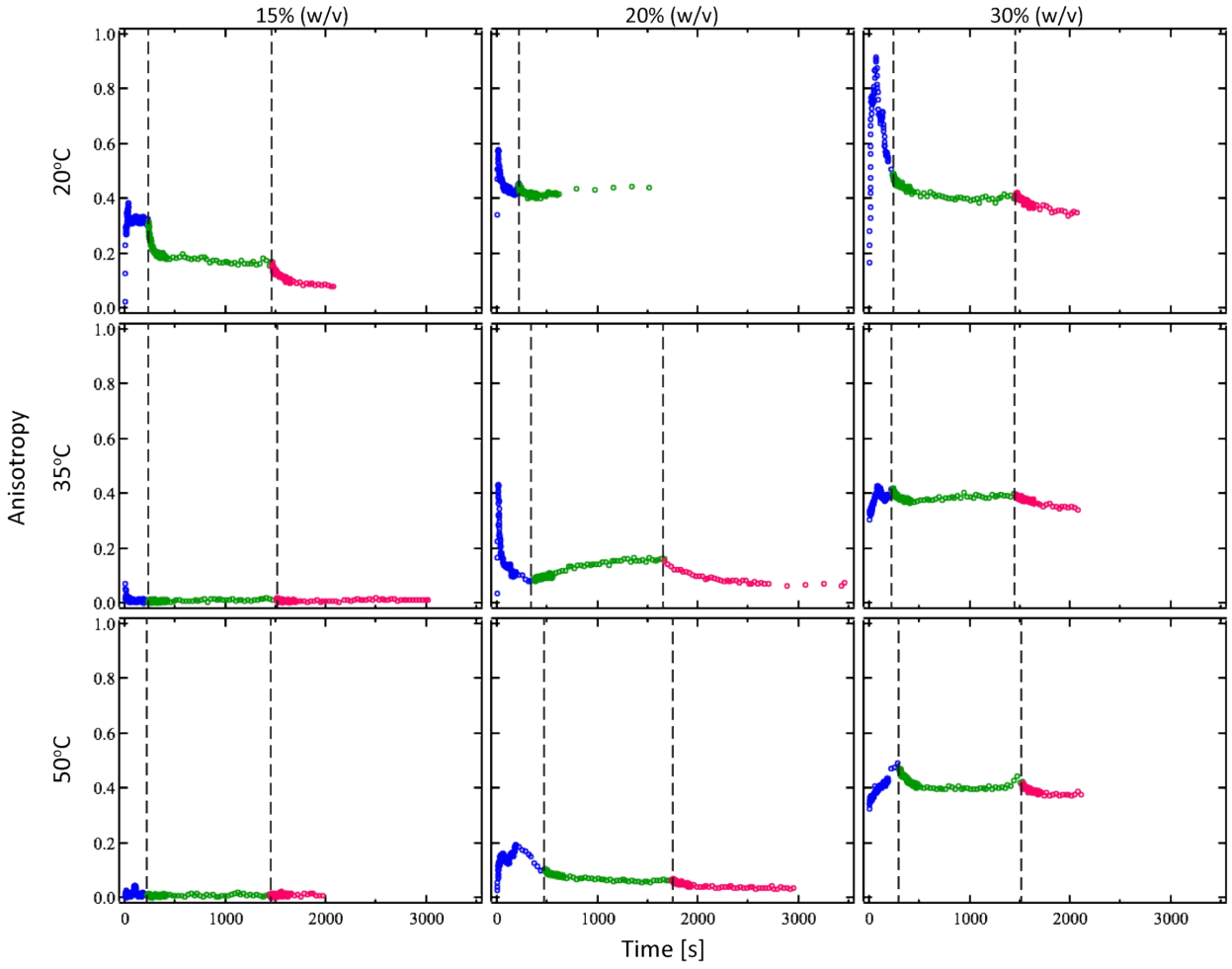

Figure S4.1: Time-dependent anisotropy values for $G_{20}P_4$ as a function of temperature and concentration. Dotted lines represent step-down in shear from 0.1 to 0.002 s^{-1} and 0.002 to 0 s^{-1}.

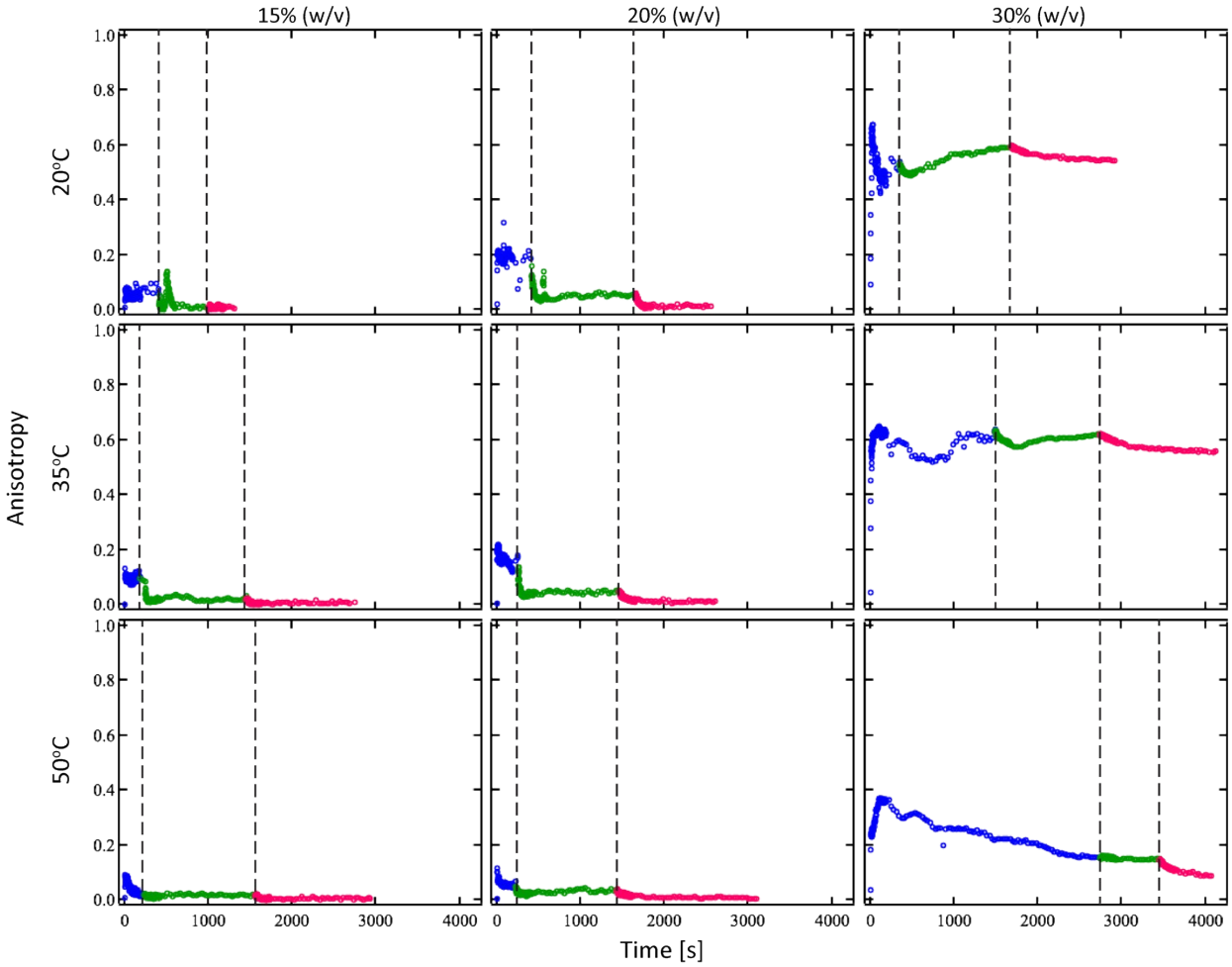

Figure S4.2: Time-dependent anisotropy values for $G_{10}P_4G_{10}$ as a function of temperature and concentration. Dotted lines represent step-down in shear from 0.1 to 0.002 s^{-1} and 0.002 to 0 s^{-1}.

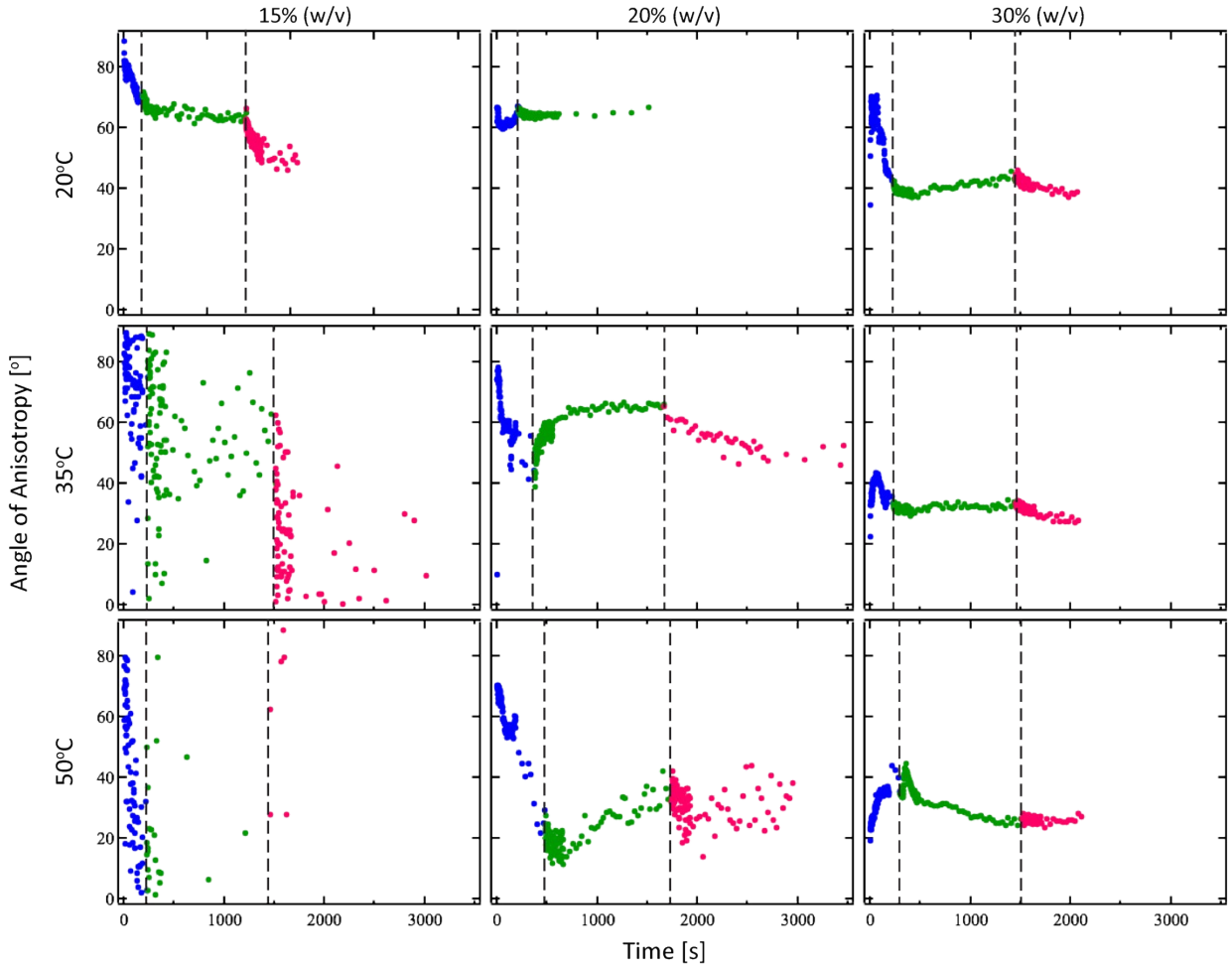

Figure S4.3: Angle of anisotropy for diblock proteins showing changes in angle as a function of concentration and temperature. Dotted lines represent step-down in shear from 0.1 to 0.002 s^{-1} and 0.002 to 0 s^{-1}.

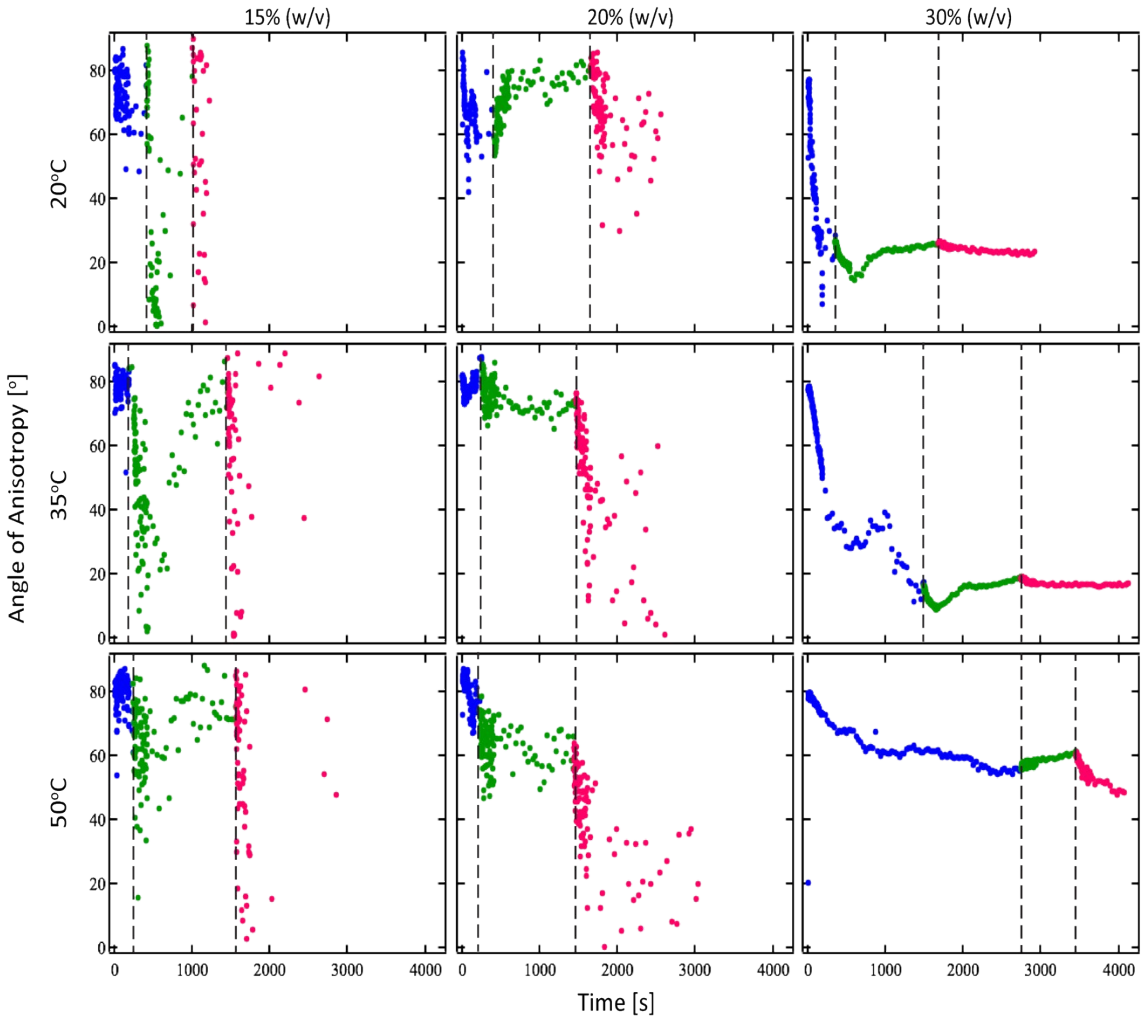

Figure S4.4: Angle of anisotropy for triblock proteins showing changes in angle as a function of concentration and temperature. Small values of anisotropy as shown in Fig. SI5 result in more noise in the angular anisotropy data. Dotted lines represent step-down in shear from 0.1 to 0.002 s^{-1} and 0.002 to 0 s^{-1}.

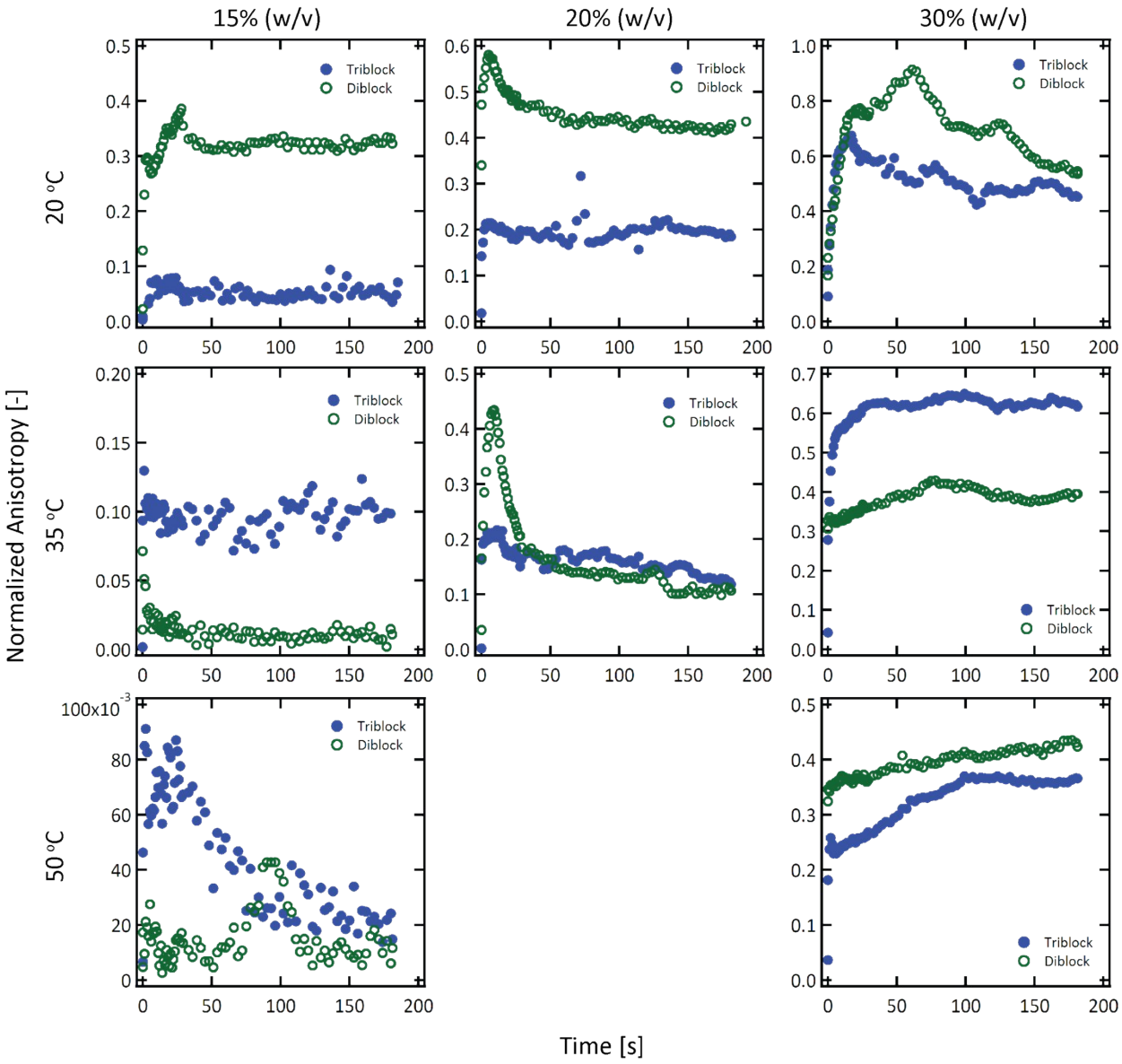

Figure S4.5: Start-up anisotropy data for both diblock and triblock proteins as a function of temperature and concentration. Note that for clarity the y-axis range was optimized on a per sample basis and are not all from 0 to 1.

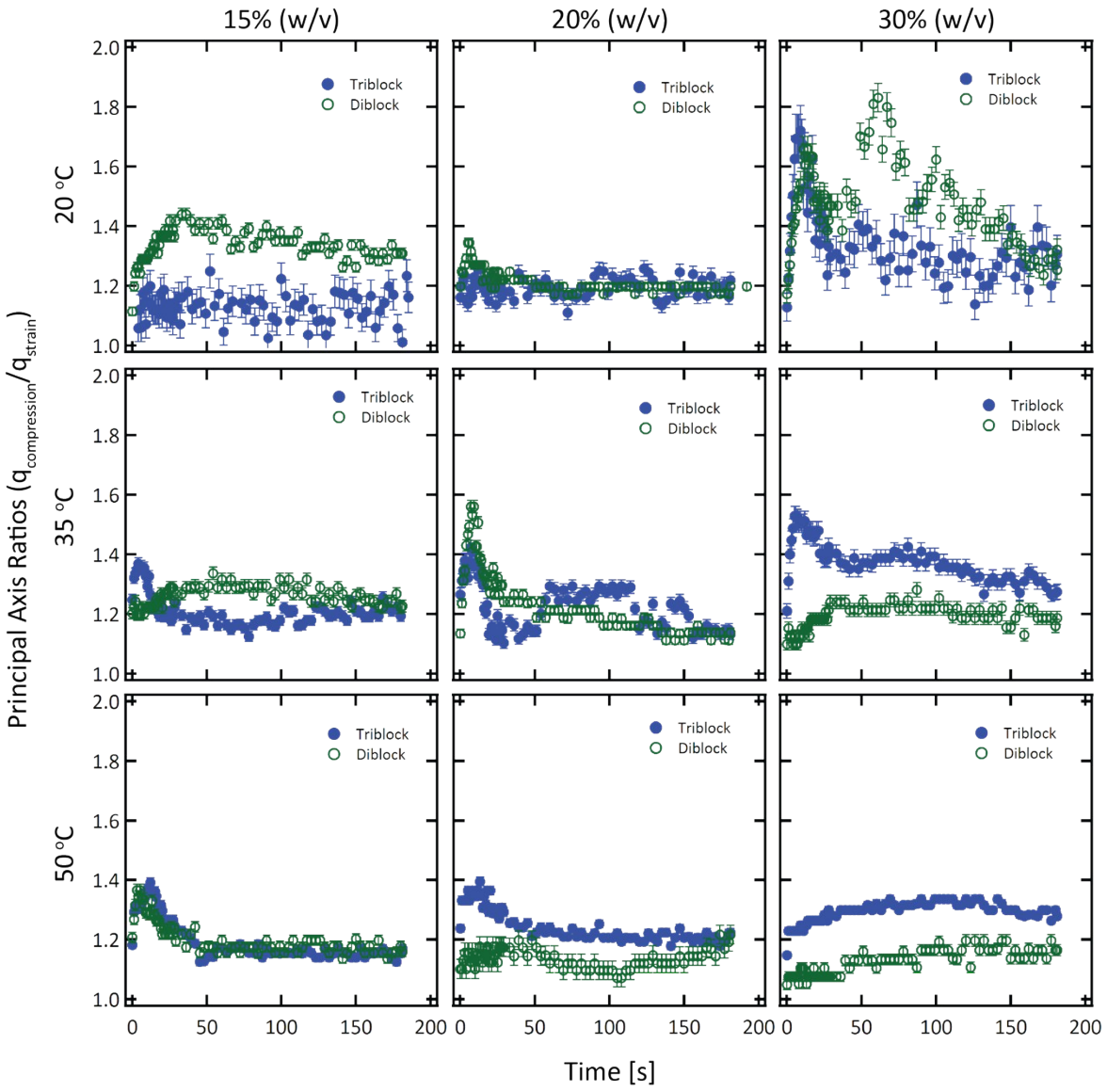

Figure S4.6: Relative deformation between diblock and triblock proteins as a function of temperature and concentration during start-up of shear. The degree of deformation was quantified using the ratio of the primary peak locations of compression and strain taken from angular slices averaged over 5˚. The principal axis of strain is rotated 45˚ away from the flow direction towards the gradient direction and the compression axis is orthogonal. The error in peak location was determined using the standard deviation of the last ten points of data (approximately 150 – 200s). The peak location was determined using Gaussian smoothing by convoluting the relevant angular slice with a Gaussian of width $\sigma = 0.01$. This smoothing is an accepted way to robustly determine the location of peaks in noisy data when the intensity is not important.[5] The peak could then be determined as the most prominent peak between the expected boundaries (0.06 and 0.2 nm^{-1} for the diblock, 0.1 and 0.25 nm^{-1} for the triblock).

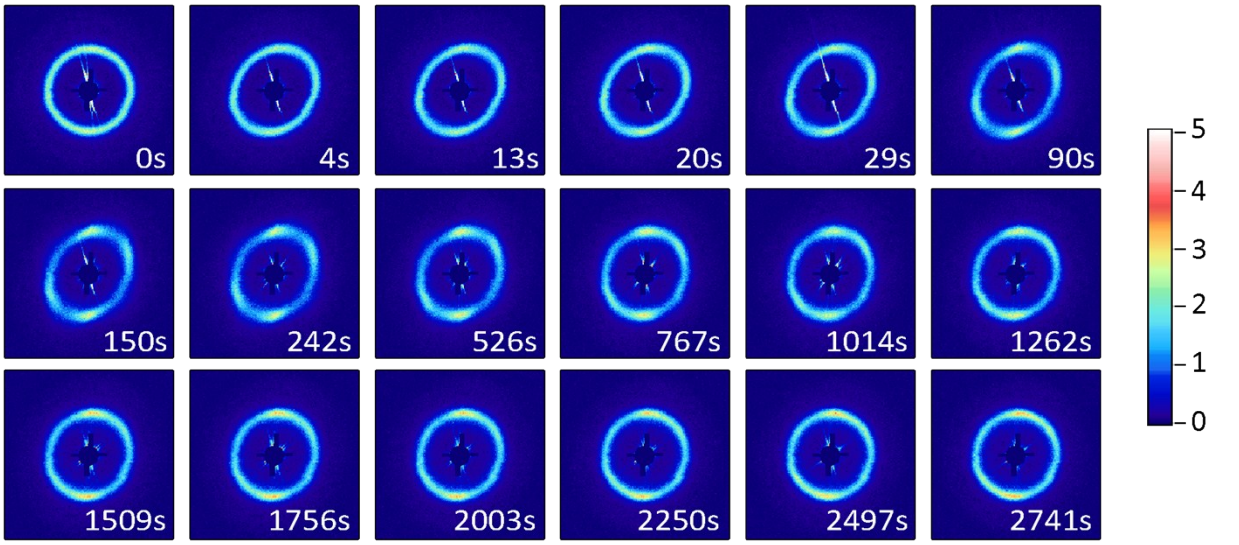

Figure S4.7: Transient 2-D scattering data for 30% (w/v) $G_{10}P_4G_{10}$ at 50 °C showing amount of time required to develop high-intensity scattering peaks along q_y relative to the same sample at 35 °C when sheared at $0.1s^{-1}$.

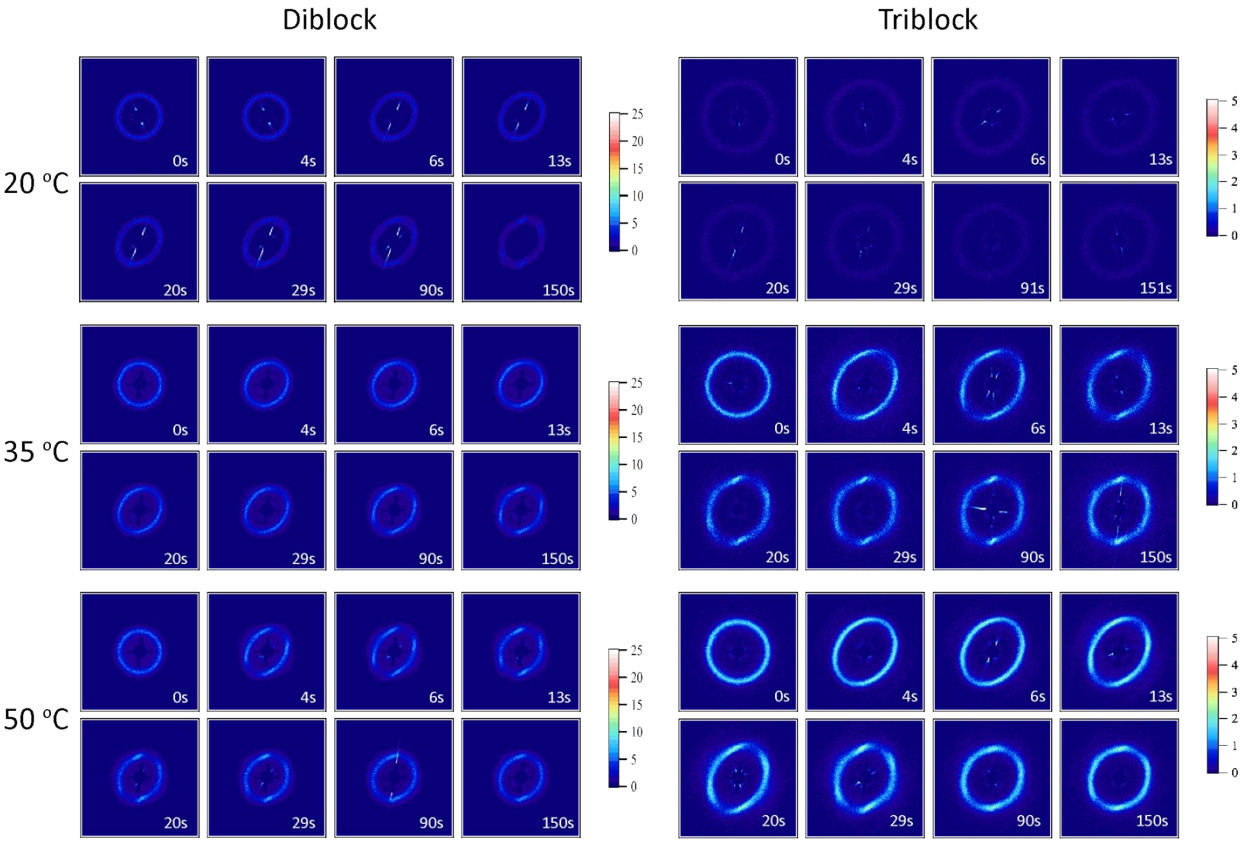

Figure S4.8: Transient start-up shear for 15% (w/v) diblock and triblock ELPs

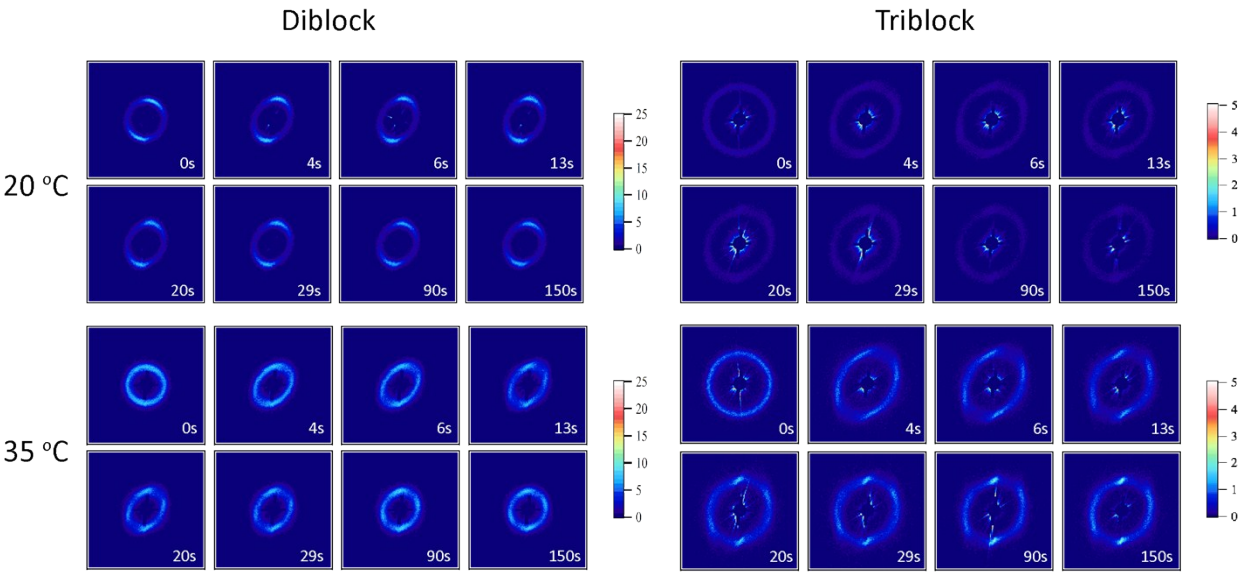

Figure S4.9: Transient start-up shear for 20% (w/v) diblock and triblock ELPs.

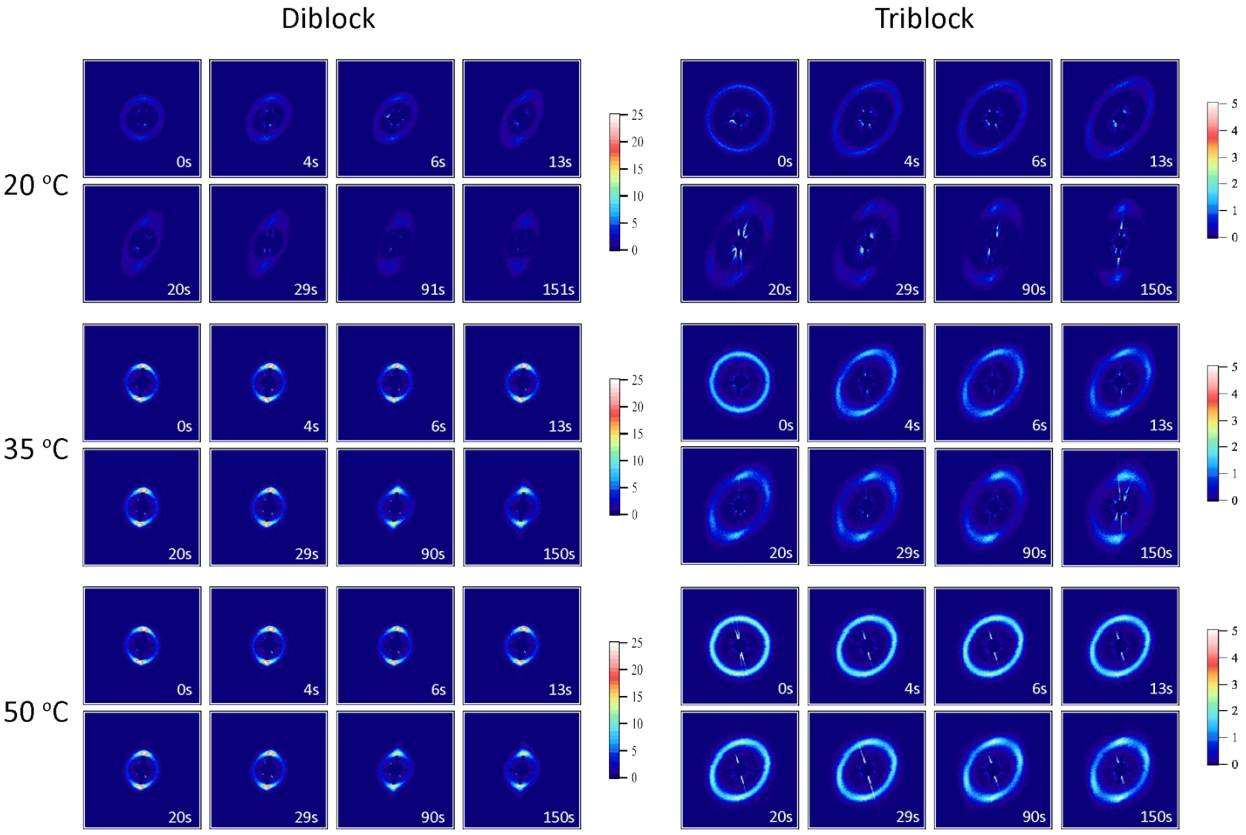

Figure S4.10: Transient start-up shear for 30% (w/v) diblock and triblock ELPs.

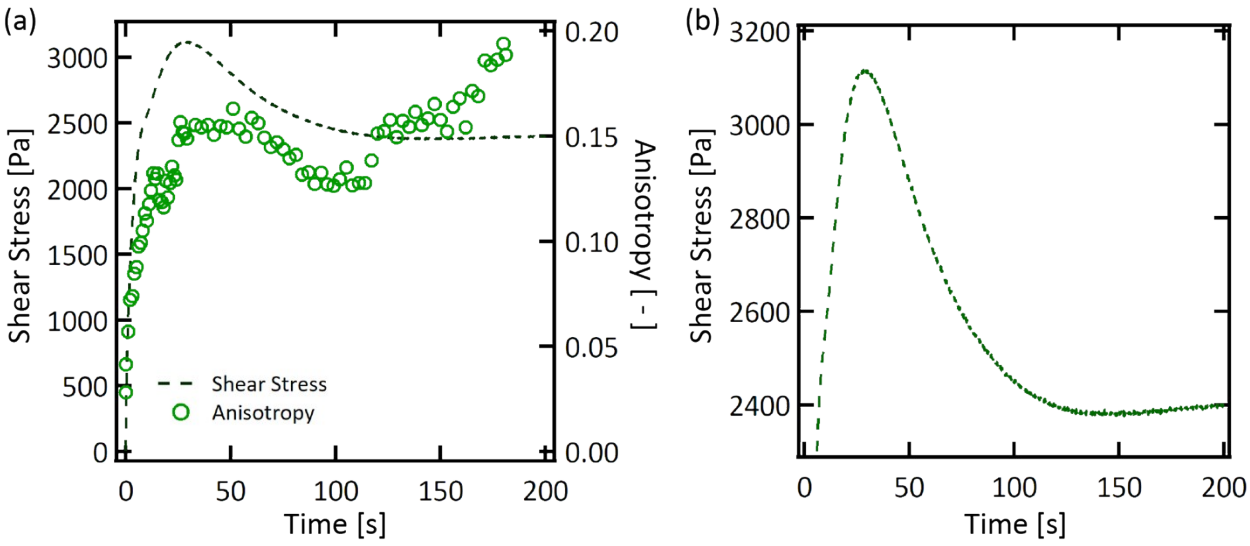

Figure S4.11: Transient start-up shear for the 20% (w/v) diblock ELP showing (a) the comparison between shear stress and the anisotropy parameter and (b) the small increase in shear stress with increasing strain following the initial overshoot.

S.5: Rheological Behavior

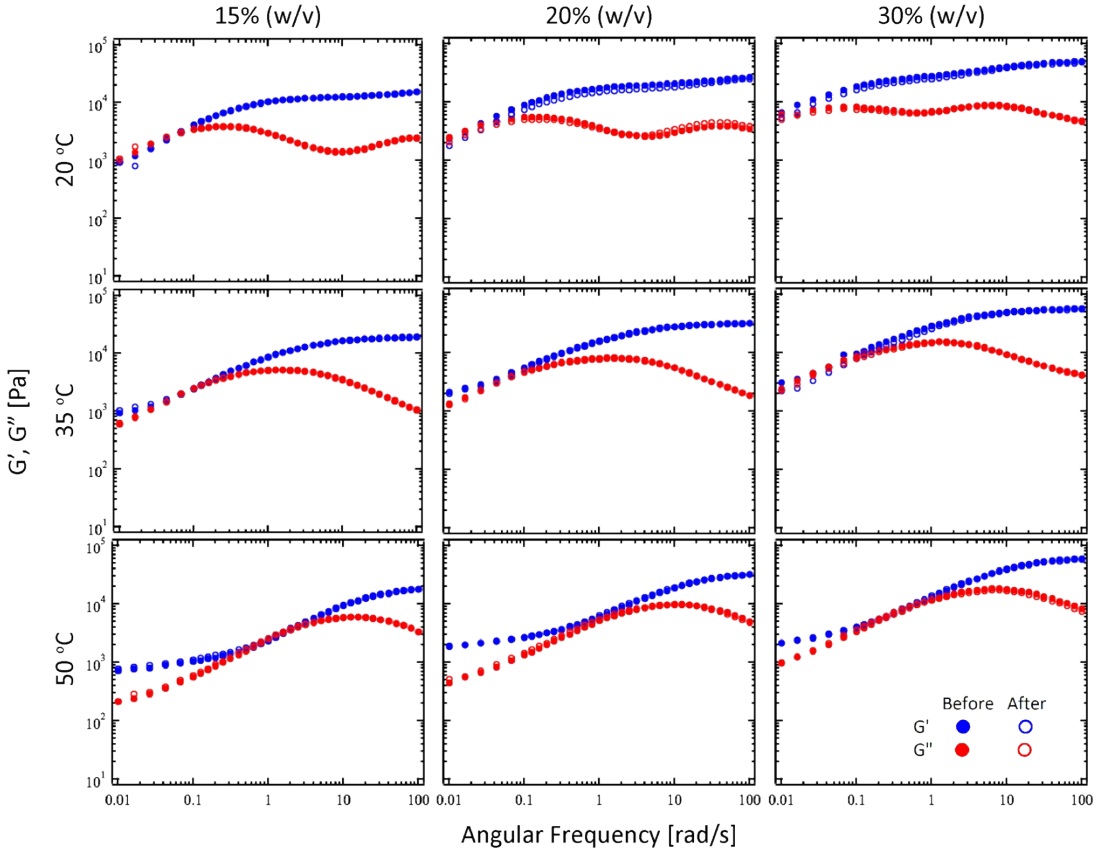

Figure S5.1: Small amplitude oscillatory shear data for $G_{20}P_4$ before and after step-shear experiments. Data taken at 1% strain with a 25 mm cone and plate.

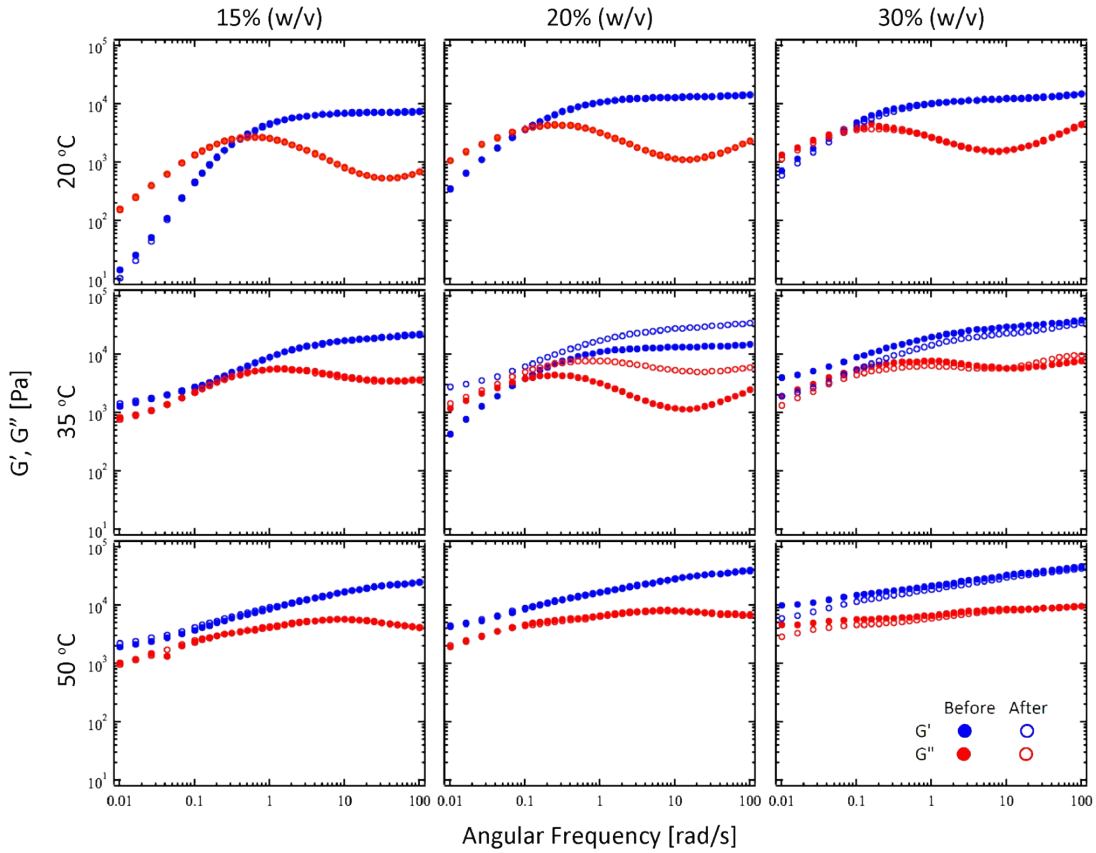

Figure S5.2: Small amplitude oscillatory shear data for $G_{10}P_4G_{10}$ as a function of temperature and concentration before and after the step-strain profile. Data was taken at 1% strain with a sandblasted 25mm cone and plate.

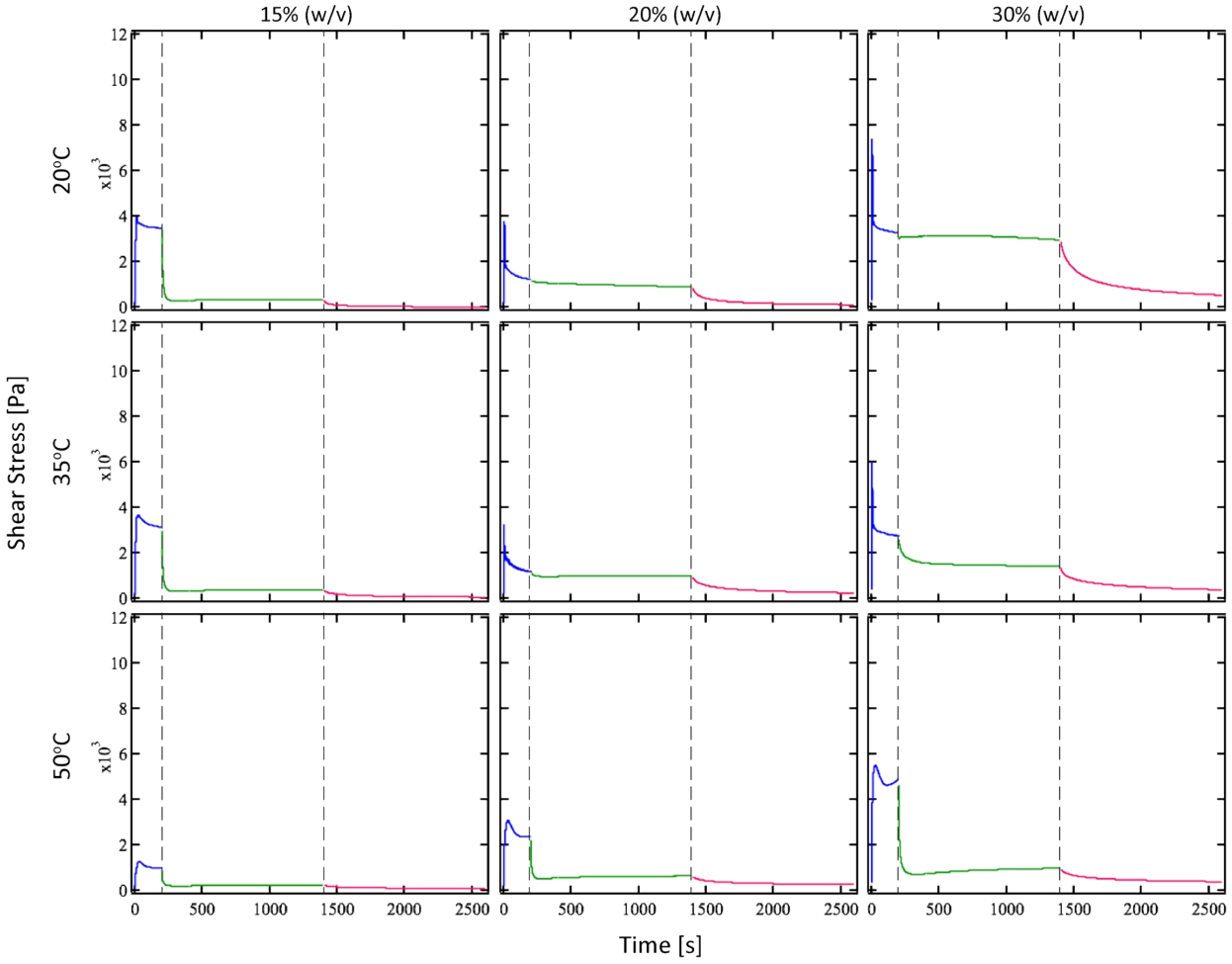

Figure S5.3: Step-shear experiments for diblock proteins as a function of concentration showing shear stress response to changes in shear rate. Dotted lines represent step-down in shear from 0.1 to 0.002 s^{-1} and 0.002 to 0 s^{-1}.

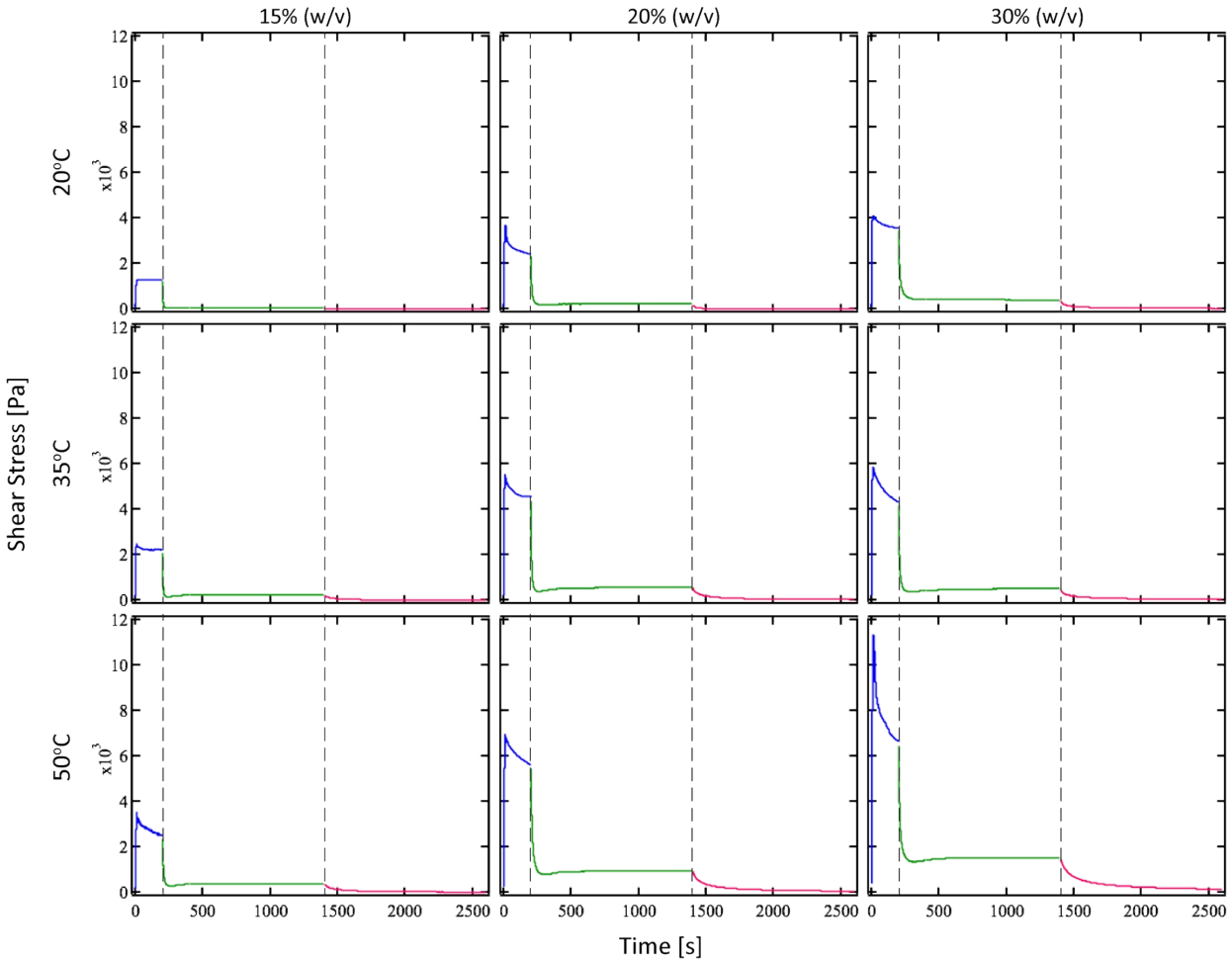

Figure S5.4: Step-shear experiments for triblock proteins as a function of concentration showing shear stress response to changes in shear rate. Dotted lines represent step-down in shear from 0.1 to 0.002 s^{-1} and 0.002 to 0 s^{-1}.

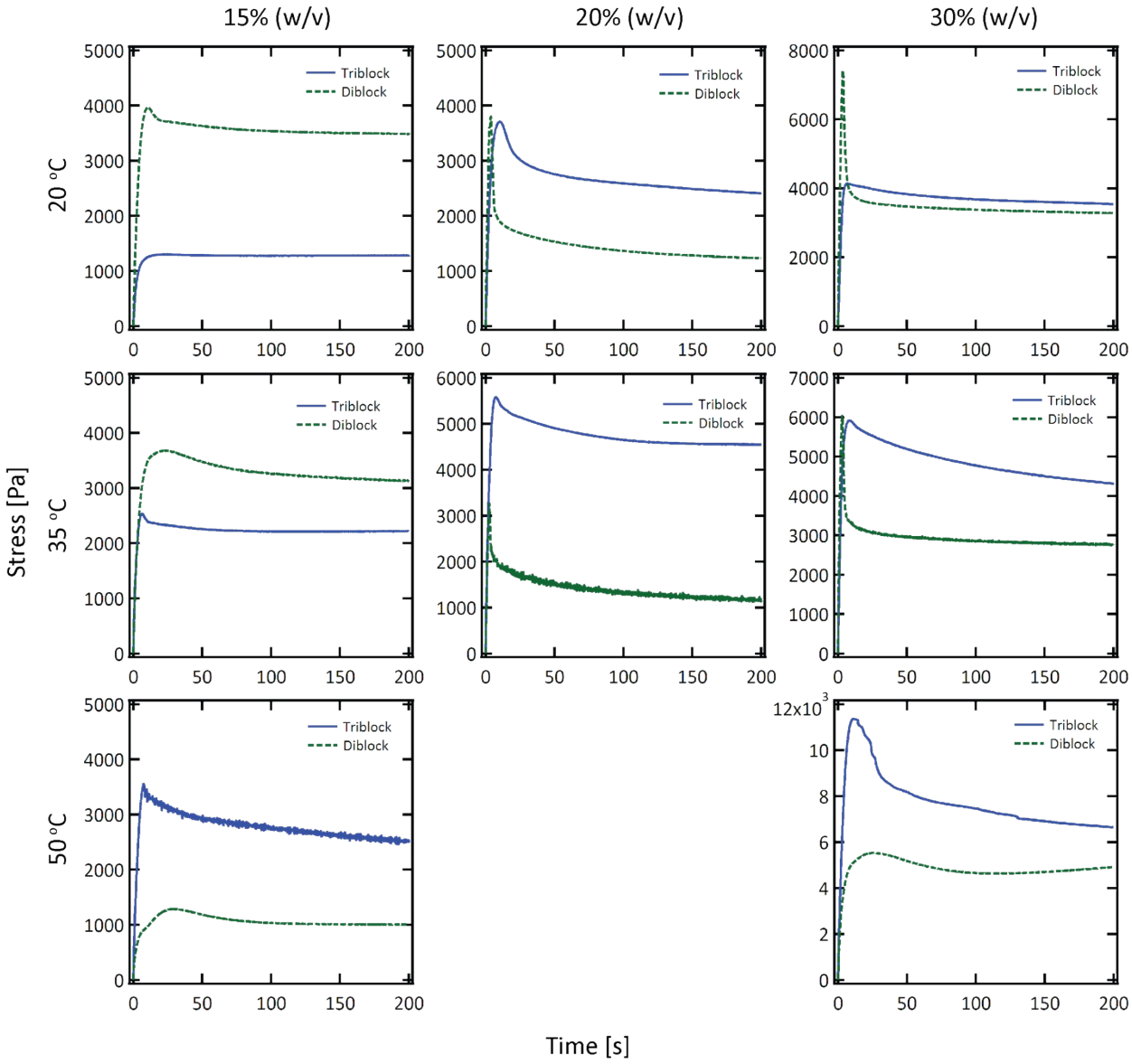

Figure S5.5: Start-up shear stress comparison for both diblock and triblock proteins as a function of temperature and concentration. Note that for clarity the y-axis range was optimized on a per sample basis and are not all identical.

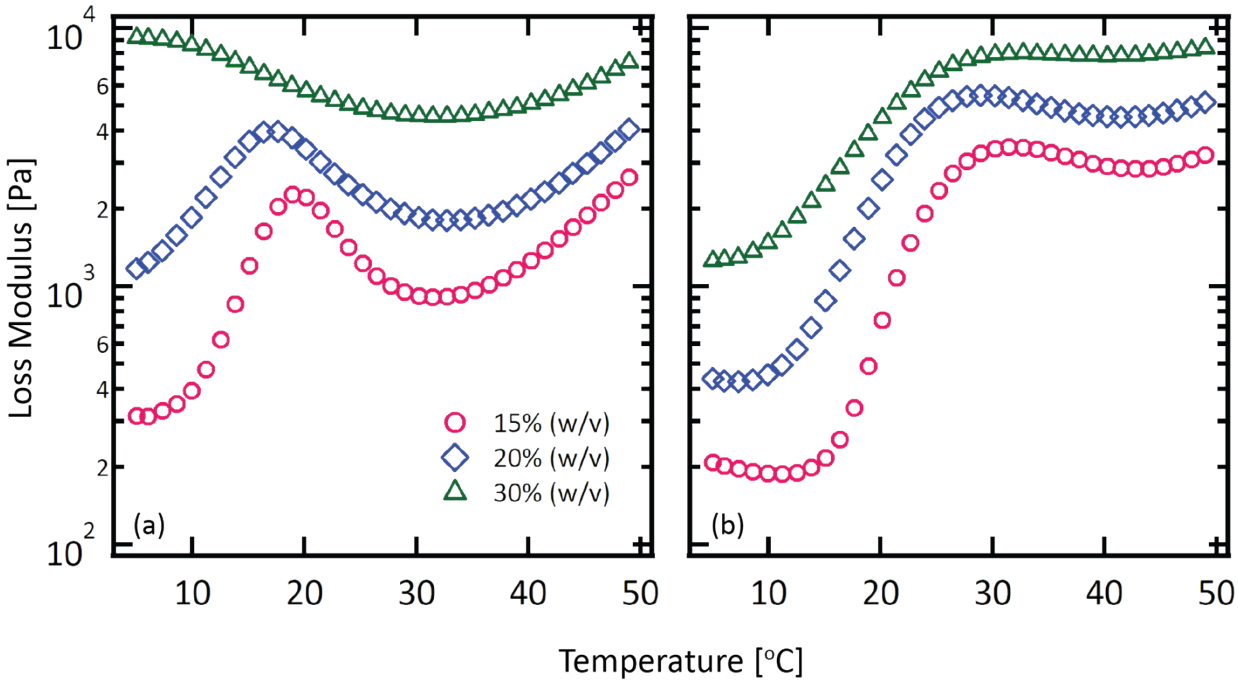

Figure S5.6: Rheology data loss moduli as a function of temperature for (a) diblock and (b) triblock as a function of gel concentration. Temperature ramps were performed at a rate of 1 °C/min while oscillating at 100 rad/s with 1% strain.

References

1. Caputo, F. E.; Burghardt, W. R.; Krishnan, K.; Bates, F. S.; Lodge, T. P., Time-resolved small-angle x-ray scattering measurements of a polymer bicontinuous microemulsion structure factor under shear. *Phys Rev E* **2002,** *66* (4).
2. Kinning, D. J.; Thomas, E. L., Hard-Sphere Interactions between Spherical Domains in Diblock Copolymers. *Macromolecules* **1984,** *17* (9), 1712-1718.
3. Percus, J. K.; Yevick, G. J., Analysis of Classical Statistical Mechanics by Means of Collective Coordinates. *Phys Rev* **1958,** *110* (1), 1-13.
4. Semenov, A. N.; Rubinstein, M., Dynamics of entangled associating polymers with large aggregates. *Macromolecules* **2002,** *35* (12), 4821-4837.
5. Trucco, E.; Verri, A., *Introductory Techniques for 3-D Computer Vision*. Prentice Hall PTR: Upper Saddle River, NJ, USA, 1998.